Detailed plasma source modeling for hydrogen masers

1st Thierry Bastin
Institut de Physique Nucléaire, Atomique et de Spectroscopie
Université de Liège
4000 Liège, Belgium
T.Bastin@uliege.be

2nd Daniel Léonard
Institut de Physique Nucléaire, Atomique et de Spectroscopie
Université de Liège
4000 Liège, Belgium
dleonard@uliege.be

***Abstract*—We report a detailed plasma source modeling for compact hydrogen masers and we show that low pressure hydrogen plasma offers better performances with respect to molecular hydrogen dissociation. The role of ions H_3^+ and H^- in the discharge plasma is also discussed.**

***Index Terms*—atomic clocks, hydrogen maser, plasma model**

I. Introduction

In a hydrogen maser atomic clock [1]–[3], a beam of state selected hydrogen atoms is sent towards a storage bulb located at the center of a cylindrical electromagnetic cavity to induce stimulated emission processes at 1420.406 MHz between the two hyperfine levels of the hydrogen atom ground state [4]. The hydrogen atoms are obtained through molecular dissociation in a standard radiofrequency (RF) discharge bulb. In this setup, the RF electromagnetic wave sustains a plasma in the bulb, where many atomic and molecular processes take place and compete, among which molecular dissociation. The experimental parameters (mainly the bulb geometry, RF injected power, molecular gas pressure in the bulb, and bulb inner surface composition) must be properly selected to optimize atomic hydrogen formation.

Here, we shall present a comprehensive global plasma modeling with a set of as much as 17 possible chemical reactions inside the plasma volume, 8 atomic and molecular hydrogen inelastic collisional processes and 4 surface reactions. The plasma particle densities for atomic and molecular hydrogen, H and H_2 respectively, as well as for all possible hydrogen ionic species, i.e., H^+, H_2^+, H_3^+ and H^-, are predicted as a function of all experimental parameters. The specific role of the ion species H_3^+ and H^- is discussed. We focus on small dissociation bulbs suited for space applications where low energy consumption is of primary importance.

II. Global plasma modeling principle

The coupling of an RF discharge with a bulb filled with molecular hydrogen H_2 results in the formation of a plasma with all possible atomic and molecular hydrogen ionic and neutral species. The volume averaged dynamics and steady state of the plasma can be computed for given experimental conditions using a so-called *plasma global model* (see for instance [5], [6]). The calculation requires to solve several

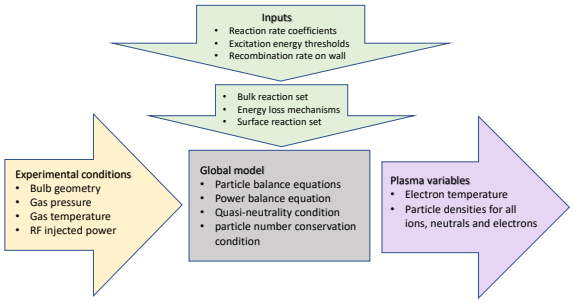

Fig. 1. Scheme of principle of a plasma global model.

standard equations. First, the *power balance equation* that expresses the balance between the RF absorbed power in the plasma with the power losses due to elastic and inelastic collisions in the plasma along with the losses due to the charged particle flow to the bulb walls. Second, the set of *particle balance equations* that express the balances per unit of time in production and loss of each species of neutrals and ions in the plasma. Third, the *quasi-neutrality condition* that expresses that the plasma is globally neutral and therefore that the sum of the electronic density with the densities of all negative ions is constantly equal to the sum of densities of all positive ions in the plasma. And finally, the *particle number conservation condition* that expresses that the weighed sum of all particle numbers reflects the total number of molecules initially in the gas that is set by the pressure.

From the set of all these equations, the dynamics and equilibrium of the plasma internal variables (densities of all neutrals – molecular and atomic – and ion species, electronic density, and electron temperature) can be computed for given experimental conditions (gas pressure p before discharge ignition, equilibrium gas temperature T, RF power P injected in the plasma, and bulb geometry). The equations are highly non-linear and such a computation requires self-consistent approaches. The equations depend on the physical mechanisms that take place within the bulb along with the rate coefficients

979-8-3503-5427-0/24/$31.00 ©2024 IEEE

1.	$e + H_2 \rightarrow H_2^+ + 2\,e$	12.	$e + H_2 \rightarrow H + H^-$
2.	$e + H_2 \rightarrow 2\,H + e$	13.	$e + H_3^+ \rightarrow H_2^+ + H^-$
3.	$e + H \rightarrow H^+ + 2e$	14.	$H^+ + H^- \rightarrow 2\,H$
4.	$H + H_2^+ \rightarrow H_2 + H^+$	15.	$H_2^+ + H^- \rightarrow 3\,H$
5.	$e + H_2^+ \rightarrow H + H^+ + e$	16.	$H_3^+ + H^- \rightarrow 4\,H$
6.	$e + H_2^+ \rightarrow 2\,H$	17.	$e + H^- \rightarrow H + 2\,e$
7.	$H_2 + H_2^+ \rightarrow H + H_3^+$		
8.	$e + H_3^+ \rightarrow 2\,H + H^+ + e$		
9.	$H_2 + H^+ \rightarrow H_3^+$		
10.	$e + H_3^+ \rightarrow 3\,H$		
11.	$e + H_3^+ \rightarrow H + H_2$		

TABLE I
REACTIONS INCLUDED IN THE MODEL ($1-6$: WITH NO H_3^+ AND H^- IONS, $7-11$: WITH H_3^+ AND NO H^- IONS, $12-17$: WITH H^- IONS).

1.	$e + H(1s) \rightarrow e + H^+ + e$
2.	$e + H(1s) \rightarrow e + H^*(n = 2, \ldots, 5)$
3.	$e + H_2(X\ ^1\Sigma_g^+) \rightarrow H_2^+ + 2\,e$
4.	$e + H_2(v = 0) \rightarrow e + H_2^*(v = 1, 2)$
5.	$e + H_2(X\ ^1\Sigma_g^+) \rightarrow e + H_2^*$ (a $^3\Sigma_g^+$, b $^3\Sigma_u^+$, c $^3\Pi_u^+$)
6.	$e + H_2(X\ ^1\Sigma_g^+) \rightarrow e + H_2^*$ (B $^1\Sigma_u^+$ $2p\sigma$)
7.	$e + H_2(X\ ^1\Sigma_g^+) \rightarrow e + H_2^*$ (C $^1\Pi_u$ $2p\pi$)
8.	$e + H_2(X\ ^1\Sigma_g^+) \rightarrow e + H_2^*$ (E,F $^1\Sigma_g^+$)

TABLE II
INELASTIC COLLISIONS CONSIDERED TO CALCULATE THE COLLISIONAL ENERGY LOSS FOR THE HYDROGEN ATOM AND MOLECULE.

1.	$H + H + \text{wall} \rightarrow H_2$
2.	$H^+ + \text{wall} \rightarrow H$
2.	$H_2^+ + \text{wall} \rightarrow H_2$
2.	$H_3^+ + \text{wall} \rightarrow H + H_2$

TABLE III
SURFACE REACTION LIST.

of these physical processes. The more reactions encoded in the model, the more elaborated it is and *a priori* the more reliable its predictions (*a priori* since this requires an accurate knowledge of the encoded reaction cross sections and the scientific literature is not always consistent nor accurate in this respect). Finally, the molecular hydrogen dissociation efficiency $\eta \equiv 1/2(N_1/N_0)$ follows from the hydrogen atomic density N_1 and the initial molecular hydrogen density before plasma ignition $N_0 = p/k_BT$, with k_B the Boltzmann constant. The scheme of principle of a plasma global model is summarized in Fig. 1.

We developed a global hydrogen plasma model with a comprehensive set of 17 bulk reactions (see Table I). The rate coefficients of the reactions where the electron is a collision partner depend on the electron temperature T_e, the others on the gas temperature T. We considered the reaction rate coefficients as explicitly listed in [5].

In the power balance equation, the only inelastic collisions in the plasma bulk that contribute significantly to the power losses are between the electrons and the neutral particles, here H and H_2 (the ion densities are too negligible for any significant contribution and can be ignored). The set of collision mechanisms that we considered for our calculations is listed in Table II. The collisional energy loss per electron-ion pair created was computed as detailed in [5].

Finally the standard set of surface reactions of Table III was considered. The negative ions H^- are supposed to remain confined in the bulk because of the negative sheath edge potential.

The rate coefficients of all inelastic and elastic collisions, as well as all surface reactions were computed according to the standard approach in a global plasma model with electronegative effects [5]. The neutralization of positive ions is extremely efficient on the surface, while the recombination of neutral hydrogen H is dependent on a recombination coefficient γ, that we set to 0.001 (standard quartz value [7]).

To validate our code, we first simulated the hydrogen plasma cell studied in [8]. In Fig. 2, we compare the steady state electron temperature T_e as a function of the gas pressure for identical experimental parameters. The curves are in excellent agreement. We observed similar excellent agreement for the predictions of the ion, neutral and electron densities in the plasma.

III. RESULTS

For compact hydrogen maser application, we simulated the plasma dynamics and steady-state for a small volume cylindrical quartz bulb of radius R = 10 mm and height L = 30 mm. Throughout our simulations, the gas temperature was set to 350 K. We first show in Fig. 3 the electron temperature T_e both as a function of the gas pressure p and the injected RF power P. The electron temperature is the real knob that tunes most rates of the different chemical reaction processes in the plasma bulk. Most of these rates drop exponentially fast for

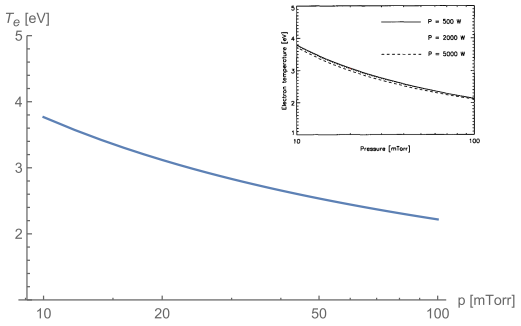

Fig. 2. Steady-state electron temperature T_e as a function of the gas pressure for the discharge cell (volume: 9.8 liters) considered in [8] (Blue: Our model with P = 500 W, inset: [8]).

T_e decreasing below 10 eV [5]. We observe that the electron temperature is almost insensitive to the injected RF power P, while it inversely depends on the gas pressure p.

The particle densities in the plasma and the dissociation efficiency η as a function of the injected RF power and the gas pressure are illustrated in Figs. 4 to 7. The ion densities are clearly negligible with respect to the neutral species densities (H and H_2) and we may write $N_2 + N_1/2 \simeq N_0$, with N_2 the molecular hydrogen density in the ignited plasma. The dissociation efficiency η thus also reads $\eta \simeq 1/(1+2N_2/N_1)$. At $\eta = 33\%$ (resp. 50%), we have $N_1 = N_2$ (resp. $N_1 = 2N_2 = N_0$). At 2 Pa, the efficiency $\eta = 33\%$ (resp. 50%) is reached for an RF power of about 1.5 W (resp. 3 W) [see Fig. 6]. At 7 W, the efficiency η reaches a value of about 70%.

At constant pressure, the electron density n_e increases linearly with the injected RF power [see Fig. 4 inset]. The reaction rates for production of atomic hydrogen (see reaction list) are mostly directly proportional to the electronic density n_e and it is therefore natural that any increase of the RF power P has a direct positive effect on the atomic hydrogen density, hence on the dissociation efficiency η (see Fig. 6).

At constant RF power, the dissociation efficiency η significantly decreases if the pressure is increased in the range $2 - 20$ Pa (see Fig. 7). This effect is similarly reported with a comparable magnitude in Refs. [5], [6], [8], where a drop of the dissociation efficiency η by a factor of about 10 is consistently reported if the gas pressure is increased from 10 to 100 mTorr (1.3 to 13 Pa) in the respective discharge cells. It has been clearly experimentally observed in the $0.4 - 4$ Pa range [9]. This can be understood as follows. The decrease of the electron temperature if the pressure is increased (Fig. 3) has a significant negative impact on atomic hydrogen production since all reactions rates are so affected. As a result, the dissociation efficiency η is negatively impacted.

In the hydrogen plasma, we can say that in the investigated range of parameters both the injected RF power P and the gas pressure p act as two efficient independent knobs on two distinct internal variables of the plasma. The RF power P forwardly tunes the electron density n_e with marginal effect on the electron temperature T_e, whereas the gas pressure p reversely tunes the electron temperature T_e, and so the hydrogen reaction rates in the bulb, with marginal effect on the electron density n_e. Both knobs act oppositely on the dissociation efficiency η: increasing the RF power P increases η (overall increase of the reactants, hence of their products), while increasing the gas pressure p decreases it (overall decrease of the reaction rates, hence of reactant products).

The computation of the dissociation efficiency η in Figures 6 and 7 has been conducted first by considering all 17 bulk chemical reaction processes of Table I (blue curves), second with only the first 11 processes, i.e., ignoring the H^- processes (orange dotted curves), and third with only the first 6 processes, i.e., ignoring both the H_3^+ and H^- processes (gray dot-dashed curves). These results clearly show that, with respect to the dissociation efficiency issue, the H^- ion processes do not play any significant role, while H_3^+ ion processes do only play a very minor role.

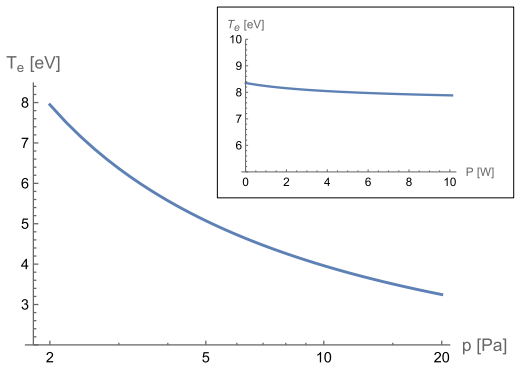

Fig. 3. Electron temperature T_e as a function of the gas pressure p (injected RF power $P = 7$ W) (Inset: as a function of the RF power at 2 Pa).

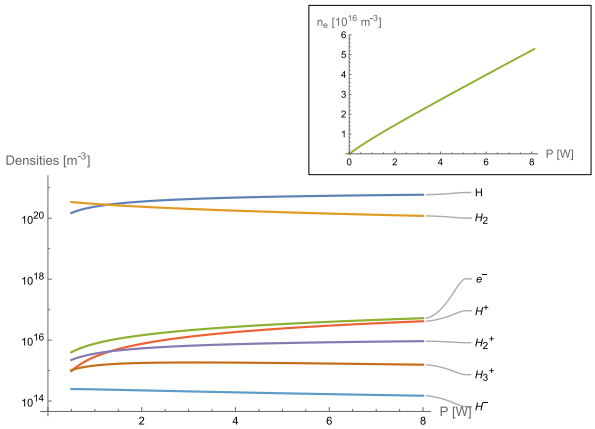

Fig. 4. Plasma particle densities as a function of the injected RF power P (gas pressure $p = 2$ Pa) (Inset: focus on the electronic density n_e).

IV. Conclusion

As a conclusion, our simulations show that in a small dissociation bulb of about 10 cm^3 very high molecular hydrogen dissociation efficiencies can be obtained at injected RF power as low as a few Watts and it is much better to operate the cell at low pressure (2 Pa for instance) than at higher pressure. In addition, we demonstrated that in the plasma cell the H^- ion processes do not play any significant role, while H_3^+ ion processes do only play a very minor role with respect to the dissociation efficiency issue. In a near future, it would be very interesting to compare quantitatively all these theoretical predictions with experimental results.

References

[1] H. M. Goldenberg, D. Kleppner, and N. F. Ramsey, "Atomic hydrogen maser," *Phys. Rev. Lett.*, vol. 5, pp. 361–362, 1960.

[2] D. Kleppner, H. M. Goldenberg, and N. F. Ramsey, "Theory of the hydrogen maser," *Phys. Rev.*, vol. 126, pp. 603–615, 1962.

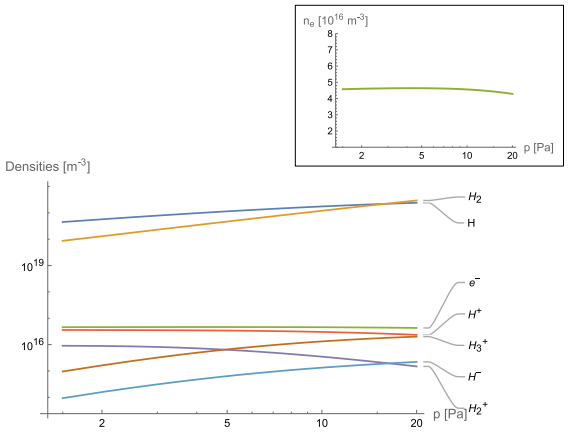

Fig. 5. Plasma particle densities as a function of the gas pressure p (injected RF power $P = 7$ W, gas temperature $T = 350$ K) (Inset: focus on the electronic density n_e).

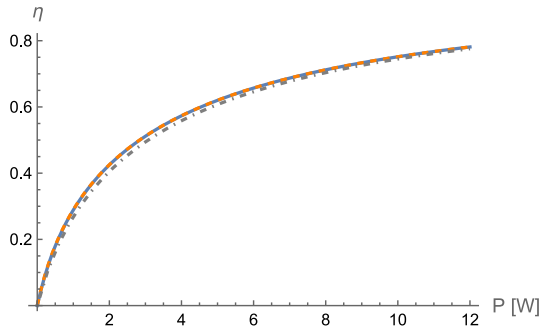

Fig. 6. Dissociation efficiency η as a function of the injected RF power P (gas pressure $p = 2$ Pa, orange dotted: only processes 1-11 of Table I [H^- ion processes ignored], gray dot-dashed: only processes 1-6 [H^- and H_3^+ ion processes ignored]).

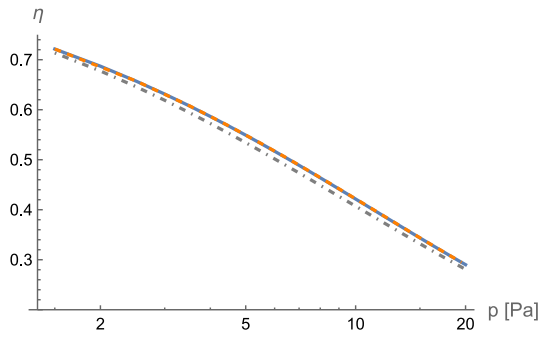

Fig. 7. Dissociation efficiency η as a function of the gas pressure p (injected RF power $P = 7$ W, orange dotted: only processes 1-11 of Table I [H^- ion processes ignored], gray dot-dashed: only processes 1-6 [H^- and H_3^+ ion processes ignored]).

[3] D. Kleppner, H. C. Berg, S. B. Crampton, *et al.*, "Hydrogen maser principles and techniques," *Phys. Rev. A*, vol. 138, pp. 972–983, 1965.

[4] J. Vanier and C. Audoin, *The Quantum Physics of Atomic Frequency Standards*. Bristol:Hilger, 1989.

[5] A. T. Hjartarson, E. G. Thorsteinsson, and J. T. Gudmundsson, "Low pressure hydrogen discharges diluted with argon explored using a global model," *Plasma Sources Sci. Technol.*, vol. 19, 065008:1–15, 2010.

[6] C. M. Samuell and C. S. Corr, "Low-pressure hydrogen plasmas explored using a global model," *Plasma Sources Sci. Technol.*, vol. 25, 015014:1–15, 2016.

[7] M. Sode, T. Schwarz-Selinger, W. Jacob, and H. Kersten, "Surface loss probability of atomic hydrogen for different electrode cover materials investigated in h_2-ar low-pressure plasmas," *J. Appl. Phys.*, vol. 116, 013302:1–10, 2014.

[8] R. Zorat, "Numerical modelling of low temperature radio-frequency hydrogen plasmas," Ph.D. dissertation, Dublin, 2003.

[9] J.-J. Dang, K.-J. Chung, and Y. S. Hwang, "A simple spectroscopic method to determine the degree of dissociation in hydrogen plasmas with wide-range spectrometer," *Rev. Scient. Instrum.*, vol. 87, 053503:1–6, 2016.